Available online at www.sciencedirect.com

ScienceDirect

Mendeleev Commun., 2023, **33**, 127–129

Mendeleev Communications

Electronic structure of carbon nanotube network

Alexander N. Ulyanov,*[a] Evgeniya V. Suslova[a] and Serguei V. Savilov[a,b]

[a] *Department of Chemistry, M. V. Lomonosov Moscow State University, 119991 Moscow, Russian Federation. E-mail: a-ulyanov52@yandex.ru*

[b] *A. V. Topchiev Institute of Petrochemical Synthesis, Russian Academy of Sciences, 119991 Moscow, Russian Federation*

DOI: 10.1016/j.mencom.2023.01.040

Covalently cross-linked carbon nanotube network has been synthesized using spark plasma sintering followed by nitric acid treatment. EPR investigation of its electronic structure in comparison with pristine carbon nanotubes has revealed that the covalent cross-linking leads to a decrease in the number of paramagnetic centers, while the oxidation results in an increase in their number. The oxidation affects the cross-linked and pristine materials in a different manner.

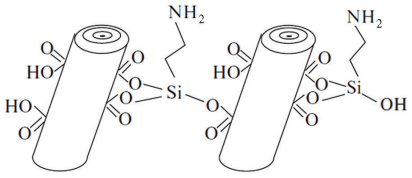

Oxidized cross-linked CNTs consolidated by SPS

Keywords: cross-linked carbon nanotubes, spark plasma sintering, electron paramagnetic resonance, X-ray photoelectron spectroscopy, transmission electron microscopy, electronic structure, charge carrier hopping mechanism.

Carbon nanomaterials (CNMs) consolidated by spark plasma sintering (SPS) are used as supercapacitor electrodes,[1] catalysts,[2] biocompatible materials[3] and adsorbents.[4] The SPS results in formation of a mesoporous structure[4] as well as improvement in electrical conductivity[5] and mechanical characteristics.[5,6] The SPS also leads to elimination of oxygen-containing groups from the bulk of material, which has been confirmed for graphene oxide,[7] electrochemically exfoliated graphite[1] and oxidized carbon nanotubes (CNTs).[8] For the effective usage of CNMs, they need to be compacted, for example, pressed and/or granulated in the presence of a binder or linked with covalent bonds.[9] Also, for most practical applications, oxygen-containing functional groups are typically generated on the surface of sintered CNMs, for instance, by treatment with a nitric acid vapor.[2] This functionalization leads to a change in the relative number of localized and mobile electrons, thus affecting the properties of CNMs.[2,10–15] Electron paramagnetic resonance (EPR) has been successfully applied to explore the interaction between delocalized and localized spins in CNMs.[10–15] Complexity and diversity of the CNMs electronic structure determine the variety of their physicochemical properties. In particular, significant number of electronic states leading to the Fermi liquid behavior were established by EPR in CNTs intercalated with potassium.[16] In this work, CNTs covalently linked by C–O–Si–O–C bridges, consolidated by the SPS and then oxidized with a nitric acid vapor were investigated by EPR.

The preparation of covalently linked CNTs (CL-CNTs)† has been described in detail.[2] We present here also a careful analysis of the samples performed by transmission electron microscopy (TEM) and X-ray photoelectron microscopy (XPS).‡ According to TEM results, the samples designated as CNT_raw, CL-CNT and CL-CNT_SPS represent multi-walled CNTs with an outer diameter of ~20 nm and inner diameter of ~8 nm [Figure 1(*a*)–(*c*)]. No visible change was observed for morphology of the three samples after their consolidation and SPS treatment. The oxidation of CL-CNT_SPS for 3 and 6 h leads to the destruction of their surface layers [Figure 1(*d*),(*e*)]. Notable, the not consolidated CNTs materials (CNT_raw, CNT_SPS,[17] CNT_SPS_3 and CNT_SPS_6[17]) consisted of well-organized nanotubes, while the oxidation for more than 6 h partially destroyed their structure. It seems that the oxidation step affects the structure of cross-linked and pristine materials differently.

XPS spectra revealed the lines of carbon, oxygen and silicon according to the system (CNT)C–O–Si–O–C(CNT) (Table 1). The SPS step leads to a significant change in the content of oxygen. According to XPS data, the SPS treatment initially results in a decrease in the oxygen content from 7.71 at% in

† CNTs were obtained by pyrolytic decomposition of hexane at 750 °C for 30 min in the presence of a Co,Mo/MgO catalyst. Then CNTs were washed by boiling in aq. HCl for 8 h. Amorphous carbon admixture was removed by annealing in air at 400 °C for 4 h. CNTs were preliminarily oxidized by boiling in aq. HNO_3 ('chemically pure' grade, Reakhim, Russia) for 4 h, the precipitate was filtered off and washed with distilled water until the neutral pH, resulting in sample(s) denoted as CNT_raw. (3-Aminopropyl)triethoxysilane (24 ml, 'chemically pure' grade) and formic acid (12 ml) were added to 50 g of CNT_raw in alcohol (250 ml) to keep the pH in the range of 4–4.5. The reaction mixture was stirred in Ar at 60 °C for 24 h, the product was washed with distilled water and dried at 60 °C for 8 h resulting in a covalently linked sample denoted as CL-CNT. SPS was performed using a Labox-625 apparatus (Sinter Land, Japan) at 1100 °C (the rate of heating 100 K min^{-1}) and an axial pressure of 30 MPa for 5 min in Graflex sheets of 2.0 mm thickness, which were then peeled off from the surface of the samples. The resulting materials were denoted as CL-CNTs_SPS. The pellets of CL-CNT_SPS were further oxidized with an HNO_3 vapor for 3.0 and 6.0 h and designated as CL-CNT_SPS_3 and CL-CNT_SPS_6, respectively.

‡ High resolution TEM images were obtained using a JEOL 2100F/Cs microscope (Japan) at accelerating voltage of 200 kV. XPS spectra were recorded on an Axis Ultra DLD instrument (Kratos Analytical, UK) using monochromatic AlKα radiation (1486.7 eV) and a pass energy of 160 eV for survey spectra and 40 eV for high resolution scans.

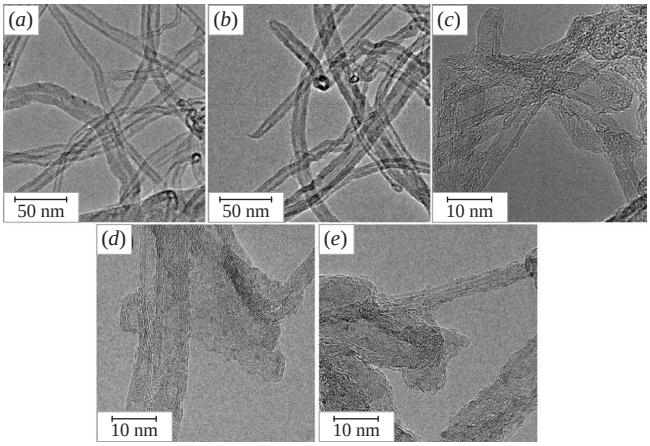

Figure 1 TEM images of the CNT samples: (*a*) CNT_raw, (*b*) CL-CNT, (*c*) CL-CNTs_SPS, (*d*) CL-CNT_SPS_3 and (*e*) CL-CNT_SPS_6. For designations, see the experiment details.

CL-CNT to 2.56 at% in CL-CNT_SPS. Subsequent oxidation increased it to 8.39 and 15.31 at% for CL-CNT_SPS_3 and CL-CNT_SPS_6, respectively. A similar trend was also observed in conventional CNTs, where the content of oxygen decreased from 1.31 at% for CNTs to 0.92 at% for CNT_SPS and then increased to 11.3 and 14.9 at% due to oxidation for 3.0 and 6.0 h in CNT_SPS_3 and CNT_SPS_6, respectively.[2] The elimination of oxygen under SPS conditions was also described for oxidized CNTs[8] and graphene oxide.[7] The original (raw) and absorption EPR spectra of the samples[§] are presented in Figure 2.

The original EPR spectra are the derivatives of the absorption ones. The signal-to-noise ratio (*S*/*N*) was equal to ~5.0, 8.0 and 11.0 for CL-CNT_SPS, CL-CNT_SPS_3 and CL-CNT_SPS_6, respectively (see Figure 2 and Table 2). Compared with our work,[2] the *S*/*N* ratios are similar to CNT_SPS_3 (~9.0), while the *S*/*N* value ~185.0 for CNT_SPS_6[2] is much higher than those obtained here. The CNT_raw and CNT_SPS samples are EPR-silent.[2,17] The EPR results allow one to make the following conclusions: (i) paramagnetic response of CL-CNT is weaker than that observed for CNTs; (ii) the oxidation time has a stronger effect on an increase in EPR signal for CNT_SPS compared with CL-CNT_SPS and (iii) an increase in paramagnetic response [that is an elevation of a number of paramagnetic centers (PMCs)] with oxidation time indicates that the PMCs are formed on unpaired electrons introduced during the oxidation step. Remarkably, paramagnetic response was not observed for CL-CNT, although the corresponding oxygen content of ~7.7 at% is higher than that for CL-CNT_SPS (~2.6 at%), in which the response was present. This means that for the appearance of an EPR signal not only the increase in the oxygen content is an important factor, but also the nature of radicals that represent the PMCs. It can be assumed that the oxygen radicals as a part of the C–O–Si–O–C covalent bridges are not PMCs and their presence does not contribute to the EPR response.

Table 1 XPS data for CL-CNT_SPS_3.

Element and XPS line	Species	Total conc. of element (at%)	Binding energy *E*/eV	Conc. of species *ν* (at%)
O1s	O=C−O	8.39	531.1	2.05
	C, H−O−C, O−Si, O−N		532.1	4.08
	O=C−O		533.1	2.26
C1s	C−C (sp^2)	90.95	284.3	86.75
	C−C, H (sp^3)		284.8	0.41
	C−O		286.5	0.98
	C=O, O−C−O		287.5	0.38
	O=C−O		288.5	2.43
Si2p	$SiO_xC_yH_z$	0.66	102.8	0.66

§ EPR measurements were conducted in the range 9.8–9.9 GHz using a Bruker EMX 6/1 spectrometer at microwave power of 0.635 mW (below the saturation power of ~2.0 mW), modulation amplitude of 1.0 G, modulation frequency of 100.00 kHz, time constant of 40.960 ms and receiver gain equal to 1.78×10^3. Background signal was subtracted using the Bruker WinEPR software. The spin numbers (*N*) of the samples were deduced using the TEMPO toluene solution as a standard with $N_{st} = 2.0792\times10^{16}$. The *N* value in the sample *i* was calculated as $N_i = (Q_{st}/Q_i)(DI_i \cdot N_{st})/DI_{st}$, where Q_{st} and Q_i are quality factors of the resonator with the standard and the sample *i*, respectively, while DI_{st} and DI_i represent the double integrated intensities of resonance curve for the standard and the sample *i*, respectively. The ratio Q_i/Q_{st} was equal to 0.95, 0.9 and 0.85 for CL-CNT_SPS, CL-CNT_SPS_3 and CL-CNT_SPS_6, respectively.

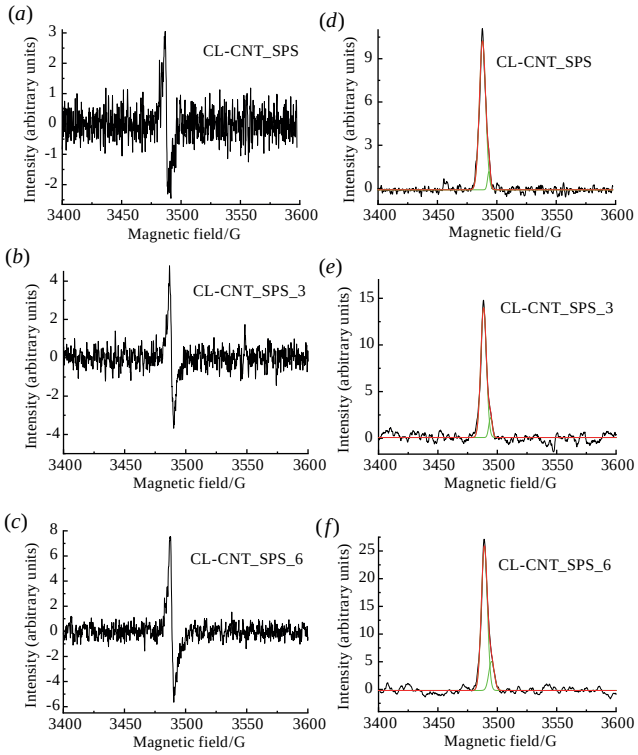

Figure 2 (*a*)–(*c*) Original and (*d*)–(*f*) absorption EPR spectra of the CNT samples.

The raw ESR spectrum lines are asymmetric reflecting the asymmetry of the absorption spectra. This in turn indicates that the spectra consist of two lines. Given the low *S*/*N* ratio, the deconvolution of the absorption spectra can only be performed roughly. The low *S*/*N* values for CNMs have already been observed and analyzed.[2,10–12] The deconvolution of absorption spectra was tried here using the Gaussian, Lorentzian and Voigt curves, the first approach gave satisfactory results. Applying the Gaussian lines, the two components were resolved in the EPR spectra of CL-CNT, resulting in an intense low field line and a weak high field one. Different *g*-factors of the lines reflect the distinct surrounding of PMCs attributed to them. All the parameters of the absorption lines are collected in Table 2 in comparison with CNT_SPS investigated in work.[2] As follows from them, the linewidth (Δ*H*) of low field line is larger than that of the high field one for CL-CNT_SPS, while it is smaller than the high field line for conventional CNT_SPS. This may be important for analysis of relative number of mobile and localized electrons in CNMs.

Table 2 EPR data for the CL-CNT_SPS and CNT_SPS samples oxidized for different time. Uncertainty in spin numbers is ~30% for all the samples except the last one, for which they are given in the table.

Sample	*S*/*N*	Linewidth ΔH/Oe		*g*-factor		Spin number $N/10^{16}$ spin g^{-1}		Source
		ΔH_{LF}[a]	ΔH_{HF}[b]	g_{LF}[a]	g_{HF}[b]	N_{LF}[a]	N_{HF}[b]	
CL-CNT_SPS	5.0	5.2(2)	2.4(4)	2.004(1)	2.001(1)	0.95	0.05	This work
CL-CNT_SPS _3	8.0	4.8(2)	3.0(3)	2.005(1)	2.002(1)	1.2	0.1	This work
CL-CNT_SPS_6	11.0	5.0(2)	4.7(3)	2.006(1)	2.002(1)	2.6	0.5	This work
CNT_SPS_3	9.0	7.5(2)	9.5(6)	2.006(1)	2.001(1)	1.5	0.4	Ref. 2
CNT_SPS_6	185.0	3.34 ± 0.03	11.77 ± 0.05	2.0060 ± 0.0002	2.0032 ± 0.0002	7.0 ± 0.4	5.5 ± 0.4	Ref. 2

[a] Low field lines. [b] High field lines.

Considering the question of whether the low field and high field lines of the absorption EPR spectra correspond to localized and/or mobile electrons, we can state the following. According to the results of graphene oxide studies,[10,11,13] the low field line is associated with mobile electrons and localized π electrons enclosed in an extended aromatic structure as well as linked to the interaction of spins, while the high field one is related to electrons localized at defects. Besides, in graphenes[18] and reduced graphene oxides[12] the high field line is attributed to mobile electrons captured by carbon vacancies in the areas separated by potential barriers, but the origin of the barriers has not been indicated. This point is important for characterization of materials. For example, in manganites the resistivity determined by scattering of electrons at the grain boundaries is higher than the resistivity inside the granule, while parameters of the corresponding EPR spectra lines are related to the properties of the grains.[19] Also, the local structure and morphology of cores and shells of granules in the manganite nanostructures differ significantly, namely, the shells represent barriers to the movement of electrons.[20] The above conclusions complement each other and correspond to the hopping mechanism of conductivity in CNMs,[10] and it is likely that electron hops can occur between PMCs belonging to both low field and high field EPR absorption lines. At present, the question stated above is still debatable. To a certain extent, this is due to a very large difference in the changes of parameters for the EPR absorption lines of CNTs,[2] graphene nanoflakes[14] and graphene oxides.[10,11,13] Note, that the results of resistivity investigation, which can shed light on electronic properties of CNMs, are also quite controversial due to the difficulty of correct measurement of the resistivity, which strongly depends on the method of sampling. The bulk samples are typically prepared from powders and their resistivity depends on the degree of compression and the homogeneity of the resulting material, in particular, its axial (in)homogeneity. It can be suggested that the observed decrease in quality factor of the resonator with the oxidizing time for CNTs originated from an increase in conductivity. Note, that there are no works where both EPR studies and resistivity measurements with comprehensive analysis of the results have been carried out for the same CNM samples.

In summary, the paramagnetic response of CL-CNT_SPS after a nitric acid vapor treatment was explored. The absorption EPR spectra can be approximated by two Gaussian lines with different *g*-factors, which indicates a distinct environment of the PMCs associated with the lines. The increase in number of PMCs with oxidation time indicates that the centers are formed as unpaired electrons introduced during the oxidation. The TEM results revealed that the oxidation process affects differently the structure of the cross-linked and pristine materials. The results are promising for the synthesis of CNTs as absorbents, materials for fuel cells and electrodes for supercapacitors as well as catalysts, biocompatible components and construction materials.

This work was supported by the Russian Science Foundation (project no. 18-13-00217). The authors thank S. V. Maksimov and K. I. Maslakov for their assistance in the TEM and XPS investigations.

References

1 Y. Gong, Y. Ping, D. Li, C. Luo, X. Ruan, Q. Fu and C. Pan, *Appl. Surf. Sci*., 2017, **397**, 213.
2 S. Savilov, E. Suslova, V. Epishev, E. Tveritinova, Y. Zhitnev, A. Ulyanov, K. Maslakov and O. Isaikina, *Nanomaterials*, 2021, **11**, 352.
3 W. Wang, A. Yokoyama, S. Liao, M. Omori, Y. Zhu, M. Uo, T. Akasaka and F. Watari, *Mater. Sci. Eng., C*, 2008, **28**, 1082.
4 C. Laurent, G. Chevallier, A. Weibel, A. Peigney and C. Estournès, *Carbon*, 2008, **46**, 1812.
5 J. L. Li, G. Z. Bai, J. W. Feng and W. Jiang, *Carbon*, 2005, **43**, 2649.
6 M. Uo, T. Tasegawa, T. Akasaka, I. Tanaka, F. Munekane, M. Omori, H. Kimura, R. Nakatomi, K. Soga, Y. Kogo and F. Watari, *Bio-Med. Mater. Eng.*, 2009, **19**, 11.
7 D. Chakravarty, C. S. Tiwary, C. F. Woellner, S. Radhakrishnan, S. Vinod, S. Ozden, P. A. da S. Autreto, S. Bhowmick, S. Asif, S. A. Mani, D. S. Galvao and P. M. Ajayan, *Adv. Mater*., 2016, **28**, 8959.
8 E. Suslova, S. Chernyak, S. Maksimov and S. Savilov, *Carbon*, 2020, **168**, 597.
9 M. Cao, C. Du, H. Guo, X. Li, S. Song, F. H. Tezel and B. Li, *Composites, Part A*, 2018, **115**, 331.
10 K. Tadyszak, K. Chybczyńska, P. Ławniczak, A. Zalewska, B. Cieniek, M. Gonet and M. Murias, *J. Magn. Magn. Mater*., 2019, **492**, 165656.
11 A. Diamantopoulou, S. Glenis, G. Zolnierkiwicz, N. Guskos and V. Likodimos, *J. Appl. Phys.*, 2017, **121**, 043906.
12 M. A. Augustyniak-Jabłokow, R. Strzelczyk and R. Fedaruk, *Carbon*, 2020, **168**, 665.
13 B. Wang, V. Likodimos, A. J. Fielding and R. A. W. Dryfe, *Carbon*, 2020, **160**, 236.
14 A. Ulyanov, D. Stolbov and S. Savilov, *Z. Phys. Chem*., 2022, **236**, 79.
15 M. Kempiński, P. Florczak, S. Jurga, M. Śliwińska-Bartkowiak and W. Kempiński, *Appl. Phys. Lett.*, 2017, **111**, 084102.
16 P. Szirmai, B. G. Márkus, B. Dóra, G. Fábián, J. Koltai, V. Zólyomi, J. Kürti, B. Náfrádi, L. Forró, T. Pichler and F. Simon, *Phys. Rev. B*, 2017, **96**, 075133.
17 A. N. Ulyanov, E. V. Suslova, K. I. Maslakov, P. K. Singh and S. V. Savilov, *Funct. Mater. Lett.*, 2022, **15**, 2251040.
18 M. A. Augustyniak-Jabłokow, K. Tadyszak, M. Maćkowiak and S. Lijewski, *Chem. Phys. Lett*., 2013, **557**, 118.
19 A. N. Ulyanov, H. D. Quang, N. E. Pismenova, S. C. Yu and G. G. Levchenko, *Solid State Commun.*, 2012, **152**, 1556.
20 A. N. Ulyanov, D. S. Yang, A. S. Mazur, V. N. Krivoruchko, G. G. Levchenko, I. A. Danilenko and T. E. Konstantinova, *J. Appl. Phys.*, 2011, **109**, 123928.

Received: 1st July 2022; Com. 22/6949